Radiotherapy and Oncology 119 (2016) 137–144

Contents lists available at ScienceDirect

Radiotherapy and Oncology

journal homepage: www.thegreenjournal.com

Review: Dual Enrgi CT

Dual energy CT in radiotherapy: Current applications and future outlook

Wouter van Elmpt [a,*], Guillaume Landry [b], Marco Das [c], Frank Verhaegen [a,d]

[a] Department of Radiation Oncology (MAASTRO), GROW – School for Oncology and Developmental Biology, Maastricht University Medical Centre, The Netherlands; [b] Department of Medical Physics, Faculty of Physics, Ludwig-Maximilians-Universität München, Garching b. München, Germany; [c] Department of Radiology, GROW – School for Oncology and Developmental Biology, Maastricht University Medical Centre, The Netherlands; and [d] Medical Physics Unit, Department of Oncology, McGill University, Montréal, Canada

ARTICLE INFO

Article history:
Received 16 October 2015
Received in revised form 13 January 2016
Accepted 28 February 2016
Available online 11 March 2016

Keywords:
Dual energy CT
Proton therapy
Brachytherapy
Dose calculation
Material decomposition

ABSTRACT

Dual energy CT (DECT) scanners are nowadays available in many radiology departments. For radiotherapy purposes, new strategies using DECT imaging are investigated to optimize radiation treatment for multiple steps in the radiotherapy chain. This review describes how DECT based methods can be used for electron density estimation, effective atomic number decomposition and contrast material quantification. Clinical radiotherapy related applications for improved dose calculation accuracy of brachytherapy and proton therapy, metal artifact reduction techniques and normal tissue characterization are also summarized together with future perspectives on the use of DECT for radiotherapy purposes.

Imaging is one of the cornerstones for diagnosis, radiation treatment planning and follow-up assessment of cancer patients. Computed tomography (CT) using X-rays is the most frequently used imaging modality for radiation therapy (RT), i.e. brachytherapy, external photon, electron and proton beam treatment [1]. Mainly the relatively easy calibration of Hounsfield Units from the CT scanner into electron density makes this modality perfectly suited for accurate dose calculation purposes in external photon beam RT. The use of other imaging modalities has increased over the past years such as magnetic resonance imaging (MRI) for regions where a high soft-tissue contrast is necessary, or functional imaging with dedicated radioactive tracers for positron emission tomography (PET). These modalities have for some treatment sites been integrated into the routine workflow for cancer patient imaging, but are nowadays typically still used in addition to CT imaging.

In recent years, the use of dual energy (DE) CT imaging has gained increased attention in radiology departments. Currently, multiple new strategies for using dual energy CT (DECT) systems for the entire chain of radiotherapy are also being investigated: e.g. improved dose calculation accuracy for brachytherapy and proton therapy, metal artifact reduction techniques and normal tissue characterization. This review article will describe the current technology available for DECT, review the possible applications and show future perspectives on the use of DECT for radiotherapy purposes.

Dual energy CT imaging: technology and physics

Imaging equipment for dual-energy CT imaging

The use of DE in CT scanners is not a recent idea. Already in the early days of CT imaging DE techniques were described [2,3]. Back then mainly technical limitations and computational power restricted the implementation of DE in routine practice. It was only a decade ago that DE imaging was introduced again, when the first clinical DECT scanner in 2005 became available [4,5]. This scanner used a dual-source technique by making use of two orthogonally-mounted X-ray tubes with corresponding detectors installed in the scanner, rotating around the patient independently operated with different kilovoltage settings. Since then, DECT has become a valuable tool in daily routine practice for different clinical mainly diagnostic applications e.g. differentiation of urinary stones, imaging of pulmonary embolism, neuro imaging or differentiation of pulmonary nodules [6–10].

Its easy use and radiation dose neutral application compared to standard routine protocols has made DECT an important new tool in daily routine practice. Furthermore, the use of DECT and further energy decomposition analysis offers a huge potential for improvement of image quality and further reduction of radiation dose [11].

* Corresponding author at: Department of Radiation Oncology (MAASTRO), GROW – School for Oncology and Developmental Biology, Maastricht University Medical Centre, Dr. Tanslaan 12, NL-6229 ET Maastricht, The Netherlands.
E-mail address: wouter.vanelmpt@maastro.nl (W. van Elmpt).

http://dx.doi.org/10.1016/j.radonc.2016.02.026
0167-8140/

The most simple approach for acquiring DE images is the rotate–rotate DE, which acquires two different scans with two different kV settings sequentially, which inherently has the disadvantage of different time points of scanning, which might be influenced by patient movement, patient breathing or different contrast media timing. Nowadays different vendors offer different solutions for DE imaging with CT [12]. As mentioned, one conceptually simple approach uses two orthogonal X-ray tubes, which are operated with two different kV settings. The X-ray tubes rotate around the patient and therefore simultaneously acquire images of different kV. Typically combinations of 80/140 kV or 100/140 kV were used, while with the latest generation even spectra of e.g. 70/150 kV are possible with the advantage of further separating the energy spectra allowing better material decomposition. Another technology uses rapid kV switching (usually in less than 0.5 ms) of the X-ray tube. Alternatively, spectral information may be obtained by a dual layer detector, which allows the detection of high and low energy photons from the same imaging beam but on two different detector layers. A recent solution available is the so called twin beam technology which offers a DE option for single source scanners by automatically splitting the X-ray beam using dedicated filters into two energy spectra at the kV source, which then expose different geometric parts of the detectors [12]. The extension of DECT from two to multiple energies by the use of photon counting detectors with energy discrimination, termed spectral CT, has been explored by investigators [13]. These systems currently exist as prototypes for pre-clinical investigation [14] and it may be necessary to further improve detector technology to compete with dual source systems [15]. An overview of the current DECT scanners is given in Supplemental Table 1.

For routine diagnostic purposes there is a strong demand for low-dose imaging and major steps in dose reduction have been achieved over the past years. One needs to keep in mind that for RT purposes the dose acquired from all imaging procedures including image-guided RT using multiple cone beam CT imaging is typically only a fraction of the dose that is delivered by the actual therapy later on [16,17]. Furthermore, with DECT imaging the dose is actually divided over the two energies used for the acquisition leading to dose levels that are approximately equal to a single energy scan [18] and acquisition of DECT images do not necessarily increase the imaging dose to the patient. However, optimization of the balance between dose burden (ALARA principle) and imaging quality should be evaluated in the RT setting which opens possibilities to optimize the acquisition protocol for the specific RT goals maximizing a benefit-to-risk ratio [19,20].

Photon attenuation coefficient decomposition

X-ray CT images are three dimensional reconstructions of the effective photon linear attenuation coefficient $\bar{\mu}$. Because of the strong energy E dependence of the linear attenuation coefficient μ and due to the poly-energetic spectra employed in X-ray CT imaging, the effective $\bar{\mu}$ is usually calculated as the sum of the contributions from photo-electric effect, Compton scattering and Rayleigh scattering to the attenuation. Whereas the photoelectric component of μ has a strong dependence on the atomic number Z, Compton scattering is governed solely by the electron density ρ_e. The attenuation coefficient allows parameterization [21], that typically can be done as functions of an effective atomic number Z_{eff} and ρ_e [3,22], as initially proposed by Hounsfield in his seminal article [2]. An example of such parameterization for $Z_{\text{eff}} < 20$ is:

$$\mu(E) = \frac{c\rho_e Z_{\text{eff}}^a}{E^b} + \sigma_{\text{KN}}(E)\rho_e + \frac{e\rho_e Z_{\text{eff}}^d}{E^f} \quad (1)$$

where a–f are best fit material and energy independent parameters and σ_{KN} is the Klein–Nishina cross section for Compton scattering [23]. While Z_{eff} and ρ_e parameterizations have an intuitive physical interpretation, any two basis functions may be employed to decompose μ. Investigators proposed to use μ of two arbitrary materials as basis functions [24,25], for example water and calcium [25]. The energy dependence of μ for the basis materials water and iodine, which are used in many applications discussed further in this review article, is illustrated in Fig. 1 together with two special purpose DECT polychromatic spectra that are produced by the X-ray tubes.

Early on, DECT basis material decomposition algorithms were divided into two main categories: projection based [3] and image based [26]. While projection based methods intrinsically correct for beam hardening effects, they require data consistency (i.e. same ray paths) between the high and low energy projections [27]. This requirement severely limits the applicability of the method to sequential scanning (due to motion) or to dual-source helical scanning where two measurements of the exact same ray-paths may not be available. Thus the image-based formalism has been employed more frequently in modern DECT implementations and we will focus on these studies in this review.

Radiotherapy interest in DECT was first raised by Devic et al. for brachytherapy applications [28]. This initial investigation estimated the linear attenuation coefficient at low photon energies from DECT; that was followed by a thorough comparison of Z_{eff} and ρ_e based parameterization to the basis material method, where the latter was found preferable for brachytherapy in terms of photon cross section estimation accuracy [23]. Other pioneering work on decomposition was based on parameterization of tabulated μ/ρ values of Bazalova et al. [29–31], which is an extension of the mono-energetic synchrotron X-ray work [32–34] to polyenergetic X-ray spectra, but requires knowledge of the X-ray spectra employed [35].

Following these initial publications several algorithms to decompose DECT images into Z_{eff} and ρ_e have been proposed [36–40]. Of practical interest are calibration-based methods where a phantom with known Z_{eff} and ρ_e in the range of human tissues is scanned and fit parameters calculated which can be used to obtain

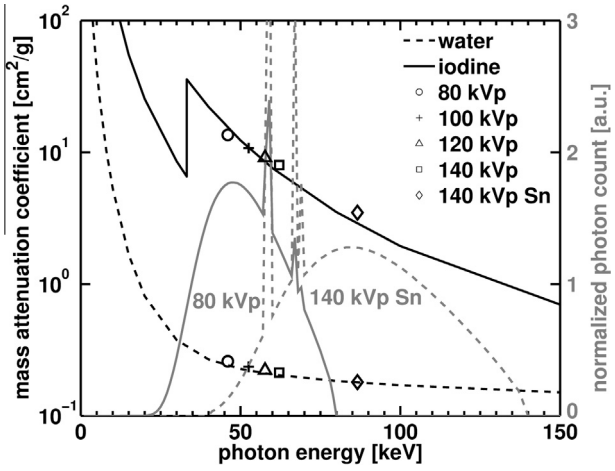

Fig. 1. Photon mass attenuation coefficients in the diagnostic imaging energy range from the NIST XCOM database [102] for the basis materials water and iodine indicated by the black dashed and solid lines, respectively. Symbols indicate the average values expected from typical X-ray spectra with various kVp generated with SpekCalc [103], plotted as a function of mean photon energy. 140 kVp Sn is filtered by tin for better spectral separation in DECT. Two typical X-ray spectra for 80 kVp and 140 kVp Sn are also shown as solid and dashed gray lines, respectively [85].

Z_{eff} and ρ_e from subsequent measurements. Saito [36] proposed a dual energy subtraction method where ρ_e is calculated with:

$$\rho_e = a\frac{[(1+\alpha)HU_H - \alpha HU_L]}{1000} + b \quad (2)$$

where a, b and α are the fit parameters and HU_H and HU_L are the CT numbers in Hounsfield units (HU) derived from the DECT images acquired at a high kVp and low kVp setting, respectively. As a reminder, CT numbers are calculated from the measured effective linear attenuation coefficient $\bar{\mu}_{meas}$ using:

$$HU = 1000\left(\frac{\bar{\mu}_{meas}}{\bar{\mu}_{water}} - 1\right) \quad (3)$$

where $\bar{\mu}_{water}$ is the effective linear attenuation coefficient of water. The accuracy of this method to derive ρ_e has been reported to be of the order of 1% [41]. A similar approach developed by Landry et al. [38] to calculate Z_{eff} is also available:

$$\frac{HU_L/1000+1}{HU_H/1000+1} = \frac{1+AZ_{eff}^{m-1}}{B+CZ_{eff}^{m-1}} \quad (4)$$

where A, B, C and m are fit parameters, reaching an accuracy of 3% for estimating Z_{eff} [38]. Similar accuracy was reported in Bourque et al. [39] for a similar phantom using a different algorithm. In terms of image noise, ρ_e is generally more robust than Z_{eff} since it is calculated by a subtraction of the two CT measurements while the latter is calculated using the ratio of the images. The level of noise on these quantities is highly dependent on the scanner type, imaging dose, spectral separation and reconstruction algorithm [20].

Contrast material quantification and mono-energetic decomposition

A decomposition of the basis vectors as described above can be used for many purposes. A frequently used parameterization to quantitatively extract the amount of contrast agent (e.g. injected iodine contrast medium) uses base pairs of water and iodine. Clinical applications of such use include quantification of lung perfusion or iodine uptake in suspected lesions. By using the basis material decomposition method, one can also virtually remove a basis material, i.e. contrast agent content, from an image and create a virtual non-contrast enhanced image. This allows both the contrast image and virtual non-contrast image being made in the same imaging session without an additional image acquisition. Contrast agents other than iodine can be used and quantified by choosing different basis material pairs. An example of this is used for lung ventilation imaging using inhaled stable xenon or krypton allowing quantification of the ventilation [42,43]. In a preclinical setting, labeled nano-particles with iodine or gold may also be effectively imaged and quantified using DECT imaging [44].

Another post-processing technique is the calculation of so-called (pseudo-)mono-chromatic (also called mono-energetic) images. An image is created by processing the dual-energy CT images to create an effective image as if it was measured using a mono-energetic beam. See Fig. 2 for an example. The image then reflects the attenuation as if it was only caused by the respective linear attenuation coefficient for the specific energy (keV) of photons. The images for these different photon energy levels should be less affected by beam hardening because of the mono-energetic beam that is reconstructed. The theoretical basis of calculating (pseudo-)monochromatic images is described in detail by Kuchenberger et al. [45]. Typically, these mono-energetic reconstructions also exhibit increased noise levels for lower keV reconstruction. Improved mono-energetic reconstruction algorithms allowing non-linear combination of the two kVp images or local spatial-frequency filtering approaches can improve the contrast-to-noise ratio [11,46,47].

Improved image quality using DE-CT

Tumor staging, delineation and characterization

Various tumors (e.g. liver, head-and-neck cancer) have a low contrast on CT imaging and therefore DECT based mono-energetic reconstructions may aid in tumor delineation. Using mono-energetic CT reconstructions at different keV settings derived from a DECT scan, images can be created with improved subjective image quality [48–50]. Although these (mainly radiological) studies showed improved subjectively and objectively quantified image quality, there is no literature yet that shows the actual delineation uncertainty used in radiotherapy planning will decrease. Another feature that could be exploited from the mono-energetic reconstructed images is the different attenuation of the lesion for the various mono-energetic energies, so-called

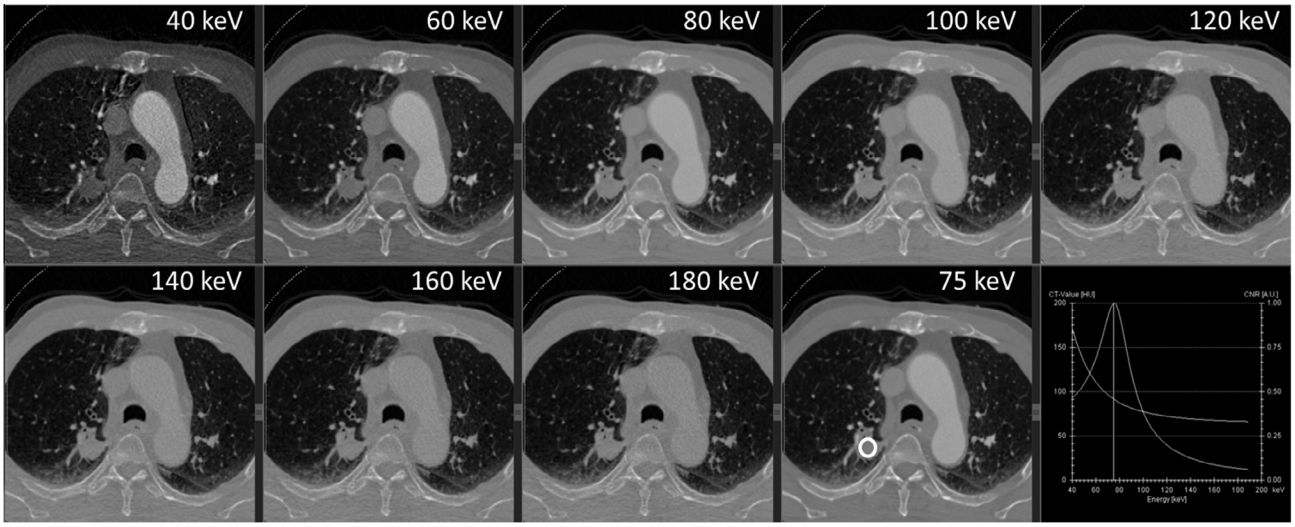

Fig. 2. Example of a mono-energetic reconstruction of a lung cancer patient. Various keV energy levels are reconstructed ranging from 40 keV to 180 keV. The bottom right panel shows the average Hounsfield Unit inside the region of interested together with an estimate of contrast-to-noise ratio, showing that 75 keV was optimal for this patient.

spectral Hounsfield Unit curves. Various authors [51,52] showed some preliminary work that allowed differentiation between benign and malignant lesions based on the characteristics of these attenuation curves. For other cancer sites such as rectal [53] or lung cancer [54–58], most papers focus on disease staging or tumor characterization using the quantification possibilities of the iodine concentration in the lesion. Although there are preliminary investigations on the use of DECT for liver tumor detection and characterization [59], there is currently no literature available on the use of DECT that evaluates the added value for delineation purposes in RT.

Normal tissue characterization

The lungs and the perfusion of lung parenchyma are frequently studied using DECT, mainly for the detection of the downstream perfusion effects of pulmonary emboli. Using material decomposition of the DECT, the distribution of intra-venously administered iodine can quantify the distribution of contrast agent inside the lung parenchyma ('perfusion'). Although this acquisition is frequently performed in a radiological setting for emboli detection it also identifies the areas with impaired lung perfusion [10]. For ventilation assessment of the lungs, inhaled contrast medium such as xenon and krypton is used [42,43,60,61]. DECT based material decomposition then allows visualization of the ventilated parts of the lung. Where other techniques such as ^{3}He MRI ventilation imaging [62,63] or perfusion imaging using 3D SPECT/CT [64,65] have been evaluated for radiotherapy treatment planning and monitoring, for DECT this is not yet fully investigated. Techniques based on DECT imaging can be incorporated in radiotherapy treatment planning to enable radiation beams passing through non-functioning lung regions, or by allowing a more quantitative evaluation of normal tissue functionality for toxicity assessment and outcome prediction [66].

DECT based metal artifact reduction strategies

Metal implants may cause streak artifacts in CT imaging, possibly hindering accurate imaging, structure delineation, electron density quantification and dose calculations in these regions. These artifacts occur mainly due to physical phenomena in CT imaging such as photon starvation, photon scatter and beam hardening. Beam hardening occurs especially for the lower photon energies and changes the spectrum of the transmitted beam. Post processing the DECT into mono-energetic images that are less affected by beam hardening was investigated to reduce these artifacts. Two studies [67,68] showed superior image quality that allowed better decision making for a variety of metallic implants for radiological purposes. The added value of mono-energetic DECT reconstructions at the highest keV reconstructions levels was most pronounced.

Comparison between three commonly used approaches for artifact reduction based on DECT with respect to other artifact reduction techniques (e.g. iterative reconstruction or frequency split techniques) shows that there is still a need for improvement of the DECT approach [45,69]. Some initial investigations comparing dose differences by using the mono-energetic approach did not lead to significant improvements. Also, the dose calculation accuracy by applying metal artifact reduction techniques solely based on a DECT principle was not significantly increased for the majority of metallic implants [70].

However, a novel approach to metal artifact reduction based on DECT that could be integrated on the imaging equipment of the linear accelerator was proposed by Wu et al. [71] to use the MV imaging beam to fill in the sinogram space of the kV cone-beam acquisition that suffered from photon starvation and artifacts.

Improved target tracking

Modern medical accelerators producing MV photons beams are equipped with an onboard kV cone beam CT unit. In principle this device could also be used for DECT imaging, but there are issues with the slow image acquisition (about 1 min/scan) and the lower image quality compared to a diagnostic CT scanner due to increased photon scatter reaching the large imaging panel. A recent phantom study used the onboard imager to acquire fast sequential DE planar X-ray images and demonstrated the benefit of bone subtraction to visualize lung tumors [72]. Imaging noise of the DE-subtracted image was ameliorated by using an anti-correlated noise reduction method [73]. In a follow-up study [74], the feasibility to enhance lung tumor visibility in patients using respiratory gated static X-ray imaging (again, not in CT mode) during treatment with external photon beams although imaging artifacts due to cardiac motion were present. Also markerless lung tumor tracking based on DE fluoroscopy has been investigated [75,76]. Phantom and pre-clinical studies showed improved DE based tracking compared to single-energy [77]. However, multiple angles might be necessary to fully assess the tumor motion in three dimensions and rapid kV switching of the imaging equipment attached to the treatment machine may be needed in clinical practice to avoid imaging artifacts and time-consuming image registration.

Improved dose calculations using DE-CT

Brachytherapy

As mentioned before, the use of DECT for brachytherapy has been advocated in several publications [20,23,28,30,78–80]. In contrast to MV photon dose calculations where knowledge of the Compton cross section, and hence the material's electron density, suffices, for brachytherapy also knowledge of the photo-electric (and to some extent, the Rayleigh coherent scatter) cross section, is important. This is particularly the case for low-energy brachytherapy with isotopes such as ^{125}I and ^{103}Pd, or electronic brachytherapy with X-ray tubes operating at 50 kVp. This implies that patient imaging should be able to extract atomic numbers of the tissue under investigation. It has been shown [81] that Monte Carlo dose calculations for low energy photons are sensitive to the tissue atomic numbers: ^{103}Pd dose calculations in breast tissue (mixture of adipose and gland) differ by up to 30% from water, and a one standard deviation from the population average breast composition adds another 10% variability [82].

While most Monte Carlo dose calculation methods require materials to be properly assigned, frequently done through their materials density and atomic number, some Monte-Carlo algorithms for photon transport require the photon interaction coefficients directly as their input. This can be performed e.g. by using Eq. (1) for decomposition into these coefficients [23,83]. Such methods were also used to calculate tissue heterogeneity correction factors for a TG43-based [84] dose calculation [78]. A series of papers [29,30,85] investigated in detail the accuracy of DECT-based extraction of electron densities and effective atomic numbers from linear attenuation coefficients to identify materials for brachytherapy dose calculation. They reported a significant improvement over tissue characterization by single energy CT (SECT). Monte Carlo dose calculations for virtual phantoms based on DECT segmentation agreed with ground truth simulation within 4% for ^{103}Pd, which is the most sensitive source to tissue misassignments (mean photon energy 21 keV). Parameterization of the ratio of high and low linear attenuation coefficients might also be used together with iterative CT reconstruction methods, which further improves the dose accuracy [20,38].

Another study [79] explored the decomposition of abdominal soft tissues into three base components: lipid, protein and water. Although they obtained unphysical negative weighting factors for many soft tissues, this approach did lead to reliable mass attenuation coefficients and mass energy absorption coefficients.

Proton therapy and verification

In proton therapy accurate estimations of the stopping power ratio (SPR), medium to water, are required by pencil beam algorithms for calculation of the proton range. Using a conversion from single energy CT images results in an uncertainty in the SPR that is a main component of the currently used treatment margin recipes [86,87]. The applicability of DECT imaging to improve the accuracy of SPR and hence proton range estimation for proton therapy treatment planning was first considered in two conference papers [31,88].

Yang et al. performed a theoretical investigation where methods to convert Z_{eff} and ρ_e to SPR for pencil beam dose calculation algorithms were presented, based on linear fits of Z_{eff} with the logarithm of the mean excitation potential [89]. They found that the accuracy and robustness of DECT for extraction of SPR was theoretically superior to SECT and could be modeled within 1% from standard human tissues values [89]. Experimental validation of these methods using phantom scans was recently presented by several investigators using modern dual source DECT scanners [37,39,40,90–93]. They reported that SPR accuracy for tissue substitutes was within 2%, compared to errors of up to 7% for SECT.

Landry et al. and Hunemohr et al. investigated the conversion of DECT images into the necessary inputs for MC simulations [94,95]. An evaluation of proton range for several tissues using SECT and DECT as input to MC simulations showed improvements in range prediction from 0.1% to 2.1% when using DECT instead of SECT [95]. An example of the difference between a proton dose calculation based on DECT and SECT is shown in Fig. 3.

Verification for proton beam delivery using positron emission tomography (PET) that rely on measurements of the decay of Carbon-11 generated during irradiation have been described [96]. Such methods depend on SECT based prediction of tissue carbon content and may suffer from inaccuracies in the assignation of tissue types [96]. Improved tissue assignment from DECT may be beneficial to this application [94] or to novel approaches currently being developed based on prompt gamma imaging [97,98] or proto-acoustics [99].

Photon therapy

The additional benefit for advanced Hounsfield Unit to electron density calibration approaches using DECT compared to single energy CT imaging for dose calculations in external beam photon therapy is limited due to the dominating Compton scattering that influences electron density estimations. Newly developed calibration schemes using a linear combination of the high and low kVp scans may allow better estimation of electron density for treatment planning, thereby reducing dose uncertainties from 11% to 1% for specific geometries [100]. Some early work was already done by Bazalova et al. showing the impact is generally around 2–3% on the dose distribution using a more accurate DECT based calibration on an 18 MV photon beam [30]. Another approach is to calculate virtual non-contrast enhanced images from a contrast-enhanced DECT scan avoiding the forcing of iodine enhanced structures for more accurate dose calculation at the planning CT scan during treatment planning [101]. This results in the advantage of having both a contrast enhanced image available for delineation purposes and a non-contrast scan for accurate dose calculation. Also, these DECT acquisitions can be performed in a dose neutral way compared to standard SECT imaging.

Concluding remarks

Dual energy CT imaging has multiple opportunities to be implemented in radiotherapy that could improve the accuracy of various parts of the workflow in the future. Starting at the stage of diagnosis, the dual energy CT imaging equipment has found its way into the radiological department and will be utilized much more in the future because of the added information that is acquired compared to single energy CT imaging in a dose-neutral way. There have been some preliminary investigations using DECT for characterization of tumor and normal tissues that are currently being investigated for implementation for improved radiotherapy for either better segmentation purposes or incorporation of DECT based functional imaging into treatment planning. The need for improved dose calculations in both brachytherapy and particle therapy worldwide is a major driver of research showing that uncertainties in the dose

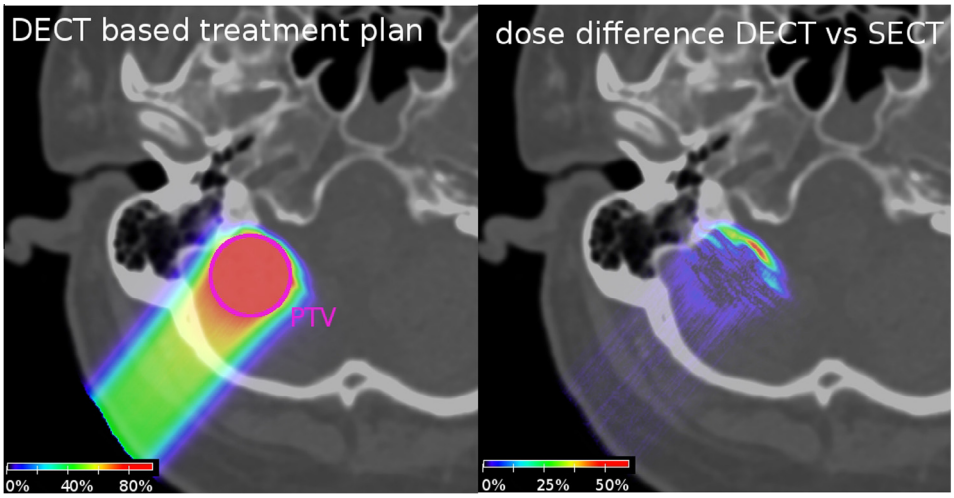

Fig. 3. Proton therapy treatment plan for a head tumor optimized on the basis of a DECT image (*left*). Absolute dose difference between the plan optimized on DECT and a plan optimized on SECT (*right*). The dose distributions of both plans were recalculated on the same image to evaluate the range difference. For both panels the color bar is in percentage of the prescription dose. Figure adapted (with permission) from Hudobivnik et al. [93].

estimation can be reduced utilizing dual energy imaging techniques.

Conflict of interest

None.

Acknowledgments

One of the authors (W.v.E.) would like to acknowledge funding (KWF MAC 2011-4970) from the Dutch Cancer Society. We would like to thank Prof. Wildberger and collaborators at Varian and Siemens for fruitful discussions. GL would like to acknowledge the support of the departments of Medical Physics (Prof. Parodi), Radiation Therapy (Prof. Belka) and Radiology (Prof. Reiser) of the LMU; in particular Prof. Sommer and Dr. Schwarz for assistance at the LMU's DECT scanners.

Appendix A. Supplementary data

Supplementary data associated with this article can be found, in the online version, at http://dx.doi.org/10.1016/j.radonc.2016.02.026.

References

[1] Grau C, Defourny N, Malicki J, Dunscombe P, Borras JM, Coffey M, et al. Radiotherapy equipment and departments in the European countries: final results from the ESTRO-HERO survey. Radiother Oncol 2014;112:155–64.
[2] Hounsfield GN. Computerized transverse axial scanning (tomography). 1. Description of system. Br J Radiol 1973;46:1016–22.
[3] Alvarez RE, Macovski A. Energy-selective reconstructions in X-ray computerized tomography. Phys Med Biol 1976;21:733–44.
[4] Johnson TR, Krauss B, Sedlmair M, Grasruck M, Bruder H, Morhard D, et al. Material differentiation by dual energy CT: initial experience. Eur Radiol 2007;17:1510–7.
[5] Petersilka M, Bruder H, Krauss B, Stierstorfer K, Flohr TG. Technical principles of dual source CT. Eur J Radiol 2008;68:362–8.
[6] Chae EJ, Song JW, Seo JB, Krauss B, Jang YM, Song KS. Clinical utility of dual-energy CT in the evaluation of solitary pulmonary nodules: initial experience. Radiology 2008;249:671–81.
[7] Graser A, Johnson TR, Bader M, Staehler M, Haseke N, Nikolaou K, et al. Dual energy CT characterization of urinary calculi: initial in vitro and clinical experience. Invest Radiol 2008;43:112–9.
[8] Okada M, Kunihiro Y, Nakashima Y, Nomura T, Kudomi S, Yonezawa T, et al. Added value of lung perfused blood volume images using dual-energy CT for assessment of acute pulmonary embolism. Eur J Radiol 2015;84:172–7.
[9] Postma AA, Das M, Stadler AA Wildberger JE. Dual-Energy CT: what the Neuroradiologist should know. Curr Radiol Rep 2015;3:16.
[10] Thieme SF, Johnson TR, Lee C, McWilliams J, Becker CR, Reiser MF, et al. Dual-energy CT for the assessment of contrast material distribution in the pulmonary parenchyma. AJR Am J Roentgenol 2009;193:144–9.
[11] Albrecht MH, Scholtz JE, Kraft J, Bauer RW, Kaup M, Dewes P, et al. Assessment of an advanced monoenergetic reconstruction technique in dual-energy computed tomography of head and neck cancer. Eur Radiol 2015;25:2493–501.
[12] Saba L, Porcu M, Schmid B Flohr T. Dual Energy CT: Basic Principles. In: De Cecco CN, Laghi A, Schoepf UJ and Meinel FG, eds. Dual Energy CT in Oncology: Springer, 2015; 1–20.
[13] Schlomka JP, Roessl E, Dorscheid R, Dill S, Martens G, Istel T, et al. Experimental feasibility of multi-energy photon-counting K-edge imaging in pre-clinical computed tomography. Phys Med Biol 2008;53:4031–47.
[14] de Vries A, Roessl E, Kneepkens E, Thran A, Brendel B, Martens G, et al. Quantitative spectral K-edge imaging in preclinical photon-counting X-ray computed tomography. Invest Radiol 2015;50:297–304.
[15] Atak H, Shikhaliev PM. Dual energy CT with photon counting and dual source systems: comparative evaluation. Phys Med Biol 2015;60:8949–75.
[16] Alaei P, Spezi E. Imaging dose from cone beam computed tomography in radiation therapy. Phys Med 2015. in press.
[17] Murphy MJ, Balter J, Balter S, BenComo Jr JA, Das IJ, Jiang SB, et al. The management of imaging dose during image-guided radiotherapy: report of the AAPM Task Group 75. Med Phys 2007;34:4041–63.
[18] Henzler T, Fink C, Schoenberg SO, Schoepf UJ. Dual-energy CT: radiation dose aspects. AJR Am J Roentgenol 2012;199:S16–25.
[19] Kalender WA. Dose in X-ray computed tomography. Phys Med Biol 2014;59:R129–50.
[20] Landry G, Gaudreault M, van Elmpt W, Wildberger JE Verhaegen F. Improved dose calculation accuracy for low energy brachytherapy by optimizing dual energy CT imaging protocols for noise reduction using sinogram affirmed iterative reconstruction. Z Med Phys 2016;26:75–87.
[21] Bornefalk H. XCOM intrinsic dimensionality for low-Z elements at diagnostic energies. Med Phys 2012;39:654–7.
[22] Rutherford RA, Pullan BR, Isherwood I. Measurement of effective atomic number and electron density using an EMI scanner. Neuroradiology 1976;11:15–21.
[23] Williamson JF, Li S, Devic S, Whiting BR, Lerma FA. On two-parameter models of photon cross sections: application to dual-energy CT imaging. Med Phys 2006;33:4115–29.
[24] Lehmann LA, Alvarez RE, Macovski A, Brody WR, Pelc NJ, Riederer SJ, et al. Generalized image combinations in dual KVP digital radiography. Med Phys 1981;8:659–67.
[25] Kalender WA, Perman WH, Vetter JR, Klotz E. Evaluation of a prototype dual-energy computed tomographic apparatus. I. Phantom studies. Med Phys 1986;13:334–9.
[26] Brooks RA. A quantitative theory of the Hounsfield unit and its application to dual energy scanning. J Comput Assist Tomogr 1977;1:487–93.
[27] Maass C, Meyer E, Kachelriess M. Exact dual energy material decomposition from inconsistent rays (MDIR). Med Phys 2011;38:691–700.
[28] Devic S, Monroe JI, Mutic S, Whiting B Williamson JF. Dual Energy CT Tissue Quantitation for Monte-Carlo Based Treatment Planning for Brachytherapy. 22nd Annual EMBS International Conference. Chicago, Il. 2000.
[29] Bazalova M, Carrier JF, Beaulieu L, Verhaegen F. Tissue segmentation in Monte Carlo treatment planning: a simulation study using dual-energy CT images. Radiother Oncol 2008;86:93–8.
[30] Bazalova M, Carrier JF, Beaulieu L, Verhaegen F. Dual-energy CT-based material extraction for tissue segmentation in Monte-Carlo dose calculations. Phys Med Biol 2008;53:2439–56.
[31] Bazalova M Verhaegen F. Tissue segmentation issues in Monte Carlo treatment planning for proton radiotherapy. PTCOG 48 conference. 2009.
[32] Torikoshi M, Tsunoo T, Sasaki M, Endo M, Noda Y, Ohno Y, et al. Electron density measurement with dual-energy X-ray CT using synchrotron radiation. Phys Med Biol 2003;48:673–85.
[33] Tsunoo T, Torikoshi M, Ohno Y, Endo M, Natsuhori M, Kakizaki T, et al. Measurement of electron density and effective atomic number using dual-energy X-ray CT. Nuclear Science Symposium Conference Record, 2004 IEEE 2004; 6: 3764–3768.
[34] Torikoshi M, Tsunoo T, Ohno Y, Endo M, Natsuhori M, Kakizaki T, et al. Features of dual-energy X-ray computed tomography. Nucl Instrum Methods Phys Res, Sect A 2005;548:99–105.
[35] Bazalova M, Verhaegen F. Monte Carlo simulation of a computed tomography X-ray tube. Phys Med Biol 2007;52:5945–55.
[36] Saito M. Potential of dual-energy subtraction for converting CT numbers to electron density based on a single linear relationship. Med Phys 2012;39:2021–30.
[37] Hunemohr N, Krauss B, Dinkel J, Gillmann C, Ackermann B, Jakel O, et al. Ion range estimation by using dual energy computed tomography. Z Med Phys 2013;23:300–13.
[38] Landry G, Seco J, Gaudreault M, Verhaegen F. Deriving effective atomic numbers from DECT based on a parameterization of the ratio of high and low linear attenuation coefficients. Phys Med Biol 2013;58:6851–66.
[39] Bourque AE, Carrier JF, Bouchard H. A stoichiometric calibration method for dual energy computed tomography. Phys Med Biol 2014;59:2059–88.
[40] Hunemohr N, Krauss B, Tremmel C, Ackermann B, Jakel O, Greilich S. Experimental verification of ion stopping power prediction from dual energy CT data in tissue surrogates. Phys Med Biol 2014;59:83–96.
[41] Tsukihara M, Noto Y, Hayakawa T, Saito M. Conversion of the energy-subtracted CT number to electron density based on a single linear relationship: an experimental verification using a clinical dual-source CT scanner. Phys Med Biol 2013;58:N135–44.
[42] Chae EJ, Seo JB, Goo HW, Kim N, Song KS, Lee SD, et al. Xenon ventilation CT with a dual-energy technique of dual-source CT: initial experience. Radiology 2008;248:615–24.
[43] Hachulla AL, Pontana F, Wemeau-Stervinou L, Khung S, Faivre JB, Wallaert B, et al. Krypton ventilation imaging using dual-energy CT in chronic obstructive pulmonary disease patients: initial experience. Radiology 2012;263:253–9.
[44] Clark DP, Ghaghada K, Moding EJ, Kirsch DG, Badea CT. In vivo characterization of tumor vasculature using iodine and gold nanoparticles and dual energy micro-CT. Phys Med Biol 2013;58:1683–704.
[45] Kuchenbecker S, Faby S, Sawall S, Lell M, Kachelriess M. Dual energy CT: how well can pseudo-monochromatic imaging reduce metal artifacts? Med Phys 2015;42:1023–36.
[46] Grant KL, Flohr TG, Krauss B, Sedlmair M, Thomas C, Schmidt B. Assessment of an advanced image-based technique to calculate virtual monoenergetic computed tomographic images from a dual-energy examination to improve contrast-to-noise ratio in examinations using iodinated contrast media. Invest Radiol 2014;49:586–92.
[47] Scholtz JE, Husers K, Kaup M, Albrecht M, Schulz B, Frellesen C, et al. Non-linear image blending improves visualization of head and neck primary squamous cell carcinoma compared to linear blending in dual-energy CT. Clin Radiol 2015;70:168–75.
[48] Wichmann JL, Noske EM, Kraft J, Burck I, Wagenblast J, Eckardt A, et al. Virtual monoenergetic dual-energy computed tomography: optimization of

kiloelectron volt settings in head and neck cancer. Invest Radiol 2014;49:735–41.
[49] Tawfik AM, Kerl JM, Bauer RW, Nour-Eldin NE, Naguib NN, Vogl TJ, et al. Dual-energy CT of head and neck cancer: average weighting of low- and high-voltage acquisitions to improve lesion delineation and image quality-initial clinical experience. Invest Radiol 2012;47:306–11.
[50] Toepker M, Czerny C, Ringl H, Fruehwald-Pallamar J, Wolf F, Weber M, et al. Can dual-energy CT improve the assessment of tumor margins in oral cancer? Oral Oncol 2014;50:221–7.
[51] Srinivasan A, Parker RA, Manjunathan A, Ibrahim M, Shah GV, Mukherji SK. Differentiation of benign and malignant neck pathologies: preliminary experience using spectral computed tomography. J Comput Assist Tomogr 2013;37:666–72.
[52] Forghani R, Levental M, Gupta R, Lam S, Dadfar N, Curtin HD. Different spectral hounsfield unit curve and high-energy virtual monochromatic image characteristics of squamous cell carcinoma compared with nonossified thyroid cartilage. AJNR Am J Neuroradiol 2015;36:1194–200.
[53] Liu H, Yan F, Pan Z, Lin X, Luo X, Shi C, et al. Evaluation of dual energy spectral CT in differentiating metastatic from non-metastatic lymph nodes in rectal cancer: Initial experience. Eur J Radiol 2015;84:228–34.
[54] Chae EJ, Song JW, Krauss B, Song KS, Lee CW, Lee HJ, et al. Dual-energy computed tomography characterization of solitary pulmonary nodules. J Thorac Imaging 2010;25:301–10.
[55] Hou WS, Wu HW, Yin Y, Cheng JJ, Zhang Q, Xu JR. Differentiation of lung cancers from inflammatory masses with dual-energy spectral CT imaging. Acad Radiol 2015;22:337–44.
[56] Lee SH, Hur J, Kim YJ, Lee HJ, Hong YJ Choi BW. Additional value of dual-energy CT to differentiate between benign and malignant mediastinal tumors: an initial experience. Eur J Radiol 2013;82:2043–9.
[57] Aoki M, Takai Y, Narita Y, Hirose K, Sato M, Akimoto H, et al. Correlation between tumor size and blood volume in lung tumors: a prospective study on dual-energy gemstone spectral CT imaging. J Radiat Res 2014;55:917–23.
[58] Schmid-Bindert G, Henzler T, Chu TQ, Meyer M, Nance Jr JW, Schoepf UJ, et al. Functional imaging of lung cancer using dual energy CT: how does iodine related attenuation correlate with standardized uptake value of 18FDG-PET-CT? Eur Radiol 2012;22:93–103.
[59] De Cecco CN, Darnell A, Macias N, Ayuso JR, Rodriguez S, Rimola J, et al. Virtual unenhanced images of the abdomen with second-generation dual-source dual-energy computed tomography: image quality and liver lesion detection. Invest Radiol 2013;48:1–9.
[60] Honda N, Osada H, Watanabe W, Nakayama M, Nishimura K, Krauss B, et al. Imaging of ventilation with dual-energy CT during breath hold after single vital-capacity inspiration of stable xenon. Radiology 2012;262:262–8.
[61] Kong X, Sheng HX, Lu GM, Meinel FG, Dyer KT, Schoepf UJ, et al. Xenon-enhanced dual-energy CT lung ventilation imaging: techniques and clinical applications. AJR Am J Roentgenol 2014;202:309–17.
[62] Hoover DA, Capaldi DP, Sheikh K, Palma DA, Rodrigues GB, Dar AR, et al. Functional lung avoidance for individualized radiotherapy (FLAIR): study protocol for a randomized, double-blind clinical trial. BMC Cancer 2014;14:934.
[63] Ireland RH, Bragg CM, McJury M, Woodhouse N, Fichele S, van Beek EJ, et al. Feasibility of image registration and intensity-modulated radiotherapy planning with hyperpolarized helium-3 magnetic resonance imaging for non-small-cell lung cancer. Int J Radiat Oncol Biol Phys 2007;68:273–81.
[64] Lavrenkov K, Singh S, Christian JA, Partridge M, Nioutsikou E, Cook G, et al. Effective avoidance of a functional spect-perfused lung using intensity modulated radiotherapy (IMRT) for non-small cell lung cancer (NSCLC): an update of a planning study. Radiother Oncol 2009;91:349–52.
[65] St-Hilaire J, Sevigny C, Beaulieu F, Germain F, Lavoie C, Dagnault A, et al. Dose escalation in the radiotherapy of non-small-cell lung cancer with aperture-based intensity modulation and photon beam energy optimization for non-preselected patients. Radiother Oncol 2009;91:342–8.
[66] Yanagita H, Honda N, Nakayama M, Watanabe W, Shimizu Y, Osada H, et al. Prediction of postoperative pulmonary function: preliminary comparison of single-breath dual-energy xenon CT with three conventional methods. Jpn J Radiol 2013;31:377–85.
[67] Bamberg F, Dierks A, Nikolaou K, Reiser MF, Becker CR, Johnson TR. Metal artifact reduction by dual energy computed tomography using monoenergetic extrapolation. Eur Radiol 2011;21:1424–9.
[68] Zhou C, Zhao YE, Luo S, Shi H, Li L, Zheng L, et al. Monoenergetic imaging of dual-energy CT reduces artifacts from implanted metal orthopedic devices in patients with factures. Acad Radiol 2011;18:1252–7.
[69] Huang JY, Kerns JR, Nute JL, Liu X, Balter PA, Stingo FC, et al. An evaluation of three commercially available metal artifact reduction methods for CT imaging. Phys Med Biol 2015;60:1047–67.
[70] Schwahofer A, Bar E, Kuchenbecker S, Grossmann JG, Kachelriess M, Sterzing F. The application of metal artifact reduction (MAR) in CT scans for radiation oncology by monoenergetic extrapolation with a DECT scanner. Z Med Phys 2015.
[71] Wu M, Keil A, Constantin D, Star-Lack J, Zhu L, Fahrig R. Metal artifact correction for X-ray computed tomography using kV and selective MV imaging. Med Phys 2014;41:121910.
[72] Hoggarth MA, Luce J, Syeda F, Bray TS, Block A, Nagda S, et al. Dual energy imaging using a clinical on-board imaging system. Phys Med Biol 2013;58:4331–40.
[73] Richard S, Siewerdsen JH. Cascaded systems analysis of noise reduction algorithms in dual-energy imaging. Med Phys 2008;35:586–601.
[74] Sherertz T, Hoggarth M, Luce J, Block AM, Nagda S, Harkenrider MM, et al. Prospective evaluation of dual-energy imaging in patients undergoing image guided radiation therapy for lung cancer: initial clinical results. Int J Radiat Oncol Biol Phys 2014;89:525–31.
[75] Patel R, Panfil J, Campana M, Block AM, Harkenrider MM, Surucu M, et al. Markerless motion tracking of lung tumors using dual-energy fluoroscopy. Med Phys 2015;42:254–62.
[76] Dhont J, Verellen D, Poels K, Tournel K, Burghelea M, Gevaert T, et al. Feasibility of markerless tumor tracking by sequential dual-energy fluoroscopy on a clinical tumor tracking system. Radiother Oncol 2015;117:487–90.
[77] Xu T, Ducote JL, Wong JT, Molloi S. Dynamic dual-energy chest radiography: a potential tool for lung tissue motion monitoring and kinetic study. Phys Med Biol 2011;56:1191–205.
[78] Mashouf S, Lechtman E, Lai P, Keller BM, Karotki A, Beachey DJ, et al. Dose heterogeneity correction for low-energy brachytherapy sources using dual-energy CT images. Phys Med Biol 2014;59:5305–16.
[79] Malusek A, Karlsson M, Magnusson M, Carlsson GA. The potential of dual-energy computed tomography for quantitative decomposition of soft tissues to water, protein and lipid in brachytherapy. Phys Med Biol 2013;58:771–85.
[80] Landry G, Granton PV, Reniers B, Ollers MC, Beaulieu L, Wildberger JE, et al. Simulation study on potential accuracy gains from dual energy CT tissue segmentation for low-energy brachytherapy Monte Carlo dose calculations. Phys Med Biol 2011;56:6257–78.
[81] Landry G, Reniers B, Murrer L, Lutgens L, Gurp EB, Pignol JP, et al. Sensitivity of low energy brachytherapy Monte Carlo dose calculations to uncertainties in human tissue composition. Med Phys 2010;37:5188–98.
[82] Woodard HQ, White DR. The composition of body tissues. Br J Radiol 1986;59:1209–18.
[83] Devic S. Dual energy CT tissue quantitation for Monte-Carlo based treatment planning for brachytherapy, 2000.
[84] Rivard MJ, Coursey BM, DeWerd LA, Hanson WF, Huq MS, Ibbott GS, et al. Update of AAPM Task Group No. 43 Report: A revised AAPM protocol for brachytherapy dose calculations. Med Phys 2004;31:633–74.
[85] Landry G, Reniers B, Granton PV, van Rooijen B, Beaulieu L, Wildberger JE, et al. Extracting atomic numbers and electron densities from a dual source dual energy CT scanner: experiments and a simulation model. Radiother Oncol 2011;100:375–9.
[86] Paganetti H. Range uncertainties in proton therapy and the role of Monte Carlo simulations. Phys Med Biol 2012;57:R99–R117.
[87] Yang M, Zhu XR, Park PC, Titt U, Mohan R, Virshup G, et al. Comprehensive analysis of proton range uncertainties related to patient stopping-power-ratio estimation using the stoichiometric calibration. Phys Med Biol 2012;57:4095–115.
[88] Beaulieu L, Bazalova M, Furstoss C, Verhaegen F. SU-FF-T-408: tissue inhomogeneities in Monte Carlo treatment planning for proton therapy. Med Phys 2009;36. 2616-2616.
[89] Yang M, Virshup G, Clayton J, Zhu XR, Mohan R, Dong L. Theoretical variance analysis of single- and dual-energy computed tomography methods for calculating proton stopping power ratios of biological tissues. Phys Med Biol 2010;55:1343–62.
[90] Farace P. Experimental verification of ion stopping power prediction from dual energy CT data in tissue surrogates. Phys Med Biol 2014;59:7081–4.
[91] Hunemohr N, Niebuhr N, Greilich S. Reply to 'Comment on "Experimental verification of ion stopping power prediction from dual energy CT data in tissue surrogates"'. Phys Med Biol 2014;59:7085–7.
[92] Hansen DC, Seco J, Sørensen TS, Petersen JBB, Wildberger JE, Verhaegen F, et al. A simulation study on proton computed tomography (CT) stopping power accuracy using dual energy CT scans as benchmark. Acta Oncol 2015:1–5.
[93] Hudobivnik N, Schwarz F, Johnson T, Agolli L, Dedes G, Tessonnier T, et al. Comparison of proton therapy treatment planning for head tumors with a pencil beam algorithm on dual and single energy CT images. Med Phys 2016;43:495.
[94] Landry G, Parodi K, Wildberger JE, Verhaegen F. Deriving concentrations of oxygen and carbon in human tissues using single- and dual-energy CT for ion therapy applications. Phys Med Biol 2013;58:5029–48.
[95] Hunemohr N, Paganetti H, Greilich S, Jakel O, Seco J. Tissue decomposition from dual energy CT data for MC based dose calculation in particle therapy. Med Phys 2014;41:061714.
[96] Parodi K, Paganetti H, Shih HA, Michaud S, Loeffler JS, DeLaney TF, et al. Patient study of in vivo verification of beam delivery and range, using positron emission tomography and computed tomography imaging after proton therapy. Int J Radiat Oncol Biol Phys 2007;68:920–34.
[97] Smeets J, Roellinghoff F, Prieels D, Stichelbaut F, Benilov A, Fiorini C, et al. Prompt gamma imaging with a slit camera for real-time range control in proton therapy. Phys Med Biol 2012;57:3371.
[98] Janssen F, Landry G, Lopes PC, Dedes G, Smeets J, Schaart D, et al. Factors influencing the accuracy of beam range estimation in proton therapy using prompt gamma emission. Phys Med Biol 2014;59:4427–41.
[99] Assmann W, Kellnberger S, Reinhardt S, Lehrack S, Edlich A, Thirolf PG, et al. Ionoacoustic characterization of the proton Bragg peak with submillimeter accuracy. Med Phys 2015;42:567–74.

[100] Tsukihara M, Noto Y, Sasamoto R, Hayakawa T, Saito M. Initial implementation of the conversion from the energy-subtracted CT number to electron density in tissue inhomogeneity corrections: an anthropomorphic phantom study of radiotherapy treatment planning. Med Phys 2015;42:1378.
[101] Yamada S, Ueguchi T, Ogata T, Mizuno H, Ogihara R, Koizumi M, et al. Radiotherapy treatment planning with contrast-enhanced computed tomography: feasibility of dual-energy virtual unenhanced imaging for improved dose calculations. Radiat Oncol 2014;9:168.
[102] Berger MJ, Hubbell JH, Seltzer SM, Chang J, Coursey JS, Sukumar R, et al. XCOM: Photon Cross Section Database (version 1.5) National Institute of Standards and Technology. Gaithersburg, MD.: Monday, 21-Dec-2015 10:39:51 EST], 2010.
[103] Poludniowski G, Landry G, DeBlois F, Evans PM, Verhaegen F. SpekCalc: a program to calculate photon spectra from tungsten anode X-ray tubes. Phys Med Biol 2009;54:N433–8.